On Frictional Forces Between the Finger and a Textured Surface During Active Touch

Marco Janko, *Student Member, IEEE,* Richard Primerano, *Member, IEEE,* and Yon Visell, *Member, IEEE*

***Abstract*—We investigated forces felt by a bare finger in sliding contact with a textured surface, and how they depend on properties of the surface and contact interaction. Prior research has shed light on haptic texture perception. Nevertheless, how texture-produced forces depend on the properties of a touched object or the way that it is touched is less clear. To address this, we designed an apparatus to accurately measure contact forces between a sliding finger and a textured surface. We fabricated textured surfaces, and measured spatial variations in forces produced as subjects explored the surfaces with a bare finger. We analyzed variations in these force signals, and their dependence on object geometry and contact parameters. We observed a number of phenomena, including transient stick-slip behavior, nonlinearities, phase variations, and large force fluctuations, in the form of aperiodic signal components that proved difficult to model for fine surfaces. Moreover, metrics such as total harmonic distortion and normalized variance decreased as the spatial scale of the stimuli increased. The results of this study suggest that surface geometry and contact parameters are insufficient to account to determine force production during such interactions. Moreover, the results shed light on perceptual challenges solved by the haptic system during active touch sensing of surface texture.**

I. Introduction

Perceiving objects via active touch is difficult because there is no simple relation between an object's properties and the mechanical stimuli delivered to the skin, which we could refer to as the "haptic appearance" of the object. How the object is oriented with respect to the fingers, how quickly it is scanned, and how contact is established and maintained also affect the mechanical stimuli. When an object's surface texture is felt, the forces that result depend on the intrinsic mechanical properties of the object, such as the geometry of the surface texture, and on factors extrinsic to the object, such as the speed of exploration or the sliding force applied (Fig. 1D).

Previous studies have demonstrated that individuals adapt their exploratory movements in ways that may improve information gained through mechanical stimuli elicited during such interactions [3], [7], [17], [35]. Prior research has lent insight into how these mechanical stimuli can be used to aid perception, how they are affected by the mechanical properties of the materials [29], [30] and finger [22], [24], and the micro and macro texture of touched surfaces [8], [9] and finger pads [5], [26], [28]. Nevertheless, the question of which aspects of mechanical stimuli are instrumental to the haptic perception of textured surfaces is still not completely understood. This is in part because we have limited knowledge of what mechanical signals are actually felt by a finger as it explores a textured surface. The present study aimed to address this gap.

From a perceptual standpoint, the duplex theory of haptic texture perception indicates that temporal variations of mechanical signals (vibrations) and spatially distributed stimulation of the skin jointly contribute to perception [13], [29], [32], [33]. Prior research has also provided evidence that reproducing the sequence of forces felt by the skin is sufficient to facilitate the perceptual identification of surface texture [21], [31], [32]. However, a small change in contact conditions can have a large effect on mechanical stimuli delivered to the finger [6], [26]. This might lead us to believe that the apparent texture of objects should vary radically, depending as much on the current conditions of contact as on the felt object. However, the fact that we can refer to objects as having surface texture indicates otherwise. As suggested by prior research [15], [16], [35], the haptic system stabilizes texture percepts against such variations. This perceptual result might be referred to as "haptic texture constancy". Although prior literature has addressed the problem of texture constancy, there is no quantitative theory for how surface properties of objects may be perceptually recovered in the face of this variability.

From an engineering viewpoint, reproducing the full range of force and displacement stimuli felt by the hand during palpation is a long term goal of haptic rendering, but, to date, we have a limited understanding of what these stimuli are. Prior methods for texture rendering have successfully employed force, displacement, or acceleration data [27], [31], but these are of limited use if we wish to simulate the experience of touching a surface that has not previously been measured, but is only known through its geometric and material specification. For example, through surface profilometry and metrology we can readily measure the physical properties of a surface, but texture display methods that are based on force sampling are unable to make use of such data. Existing physically-motivated approaches to using surface specifications to compute forces between a rigid tool and a virtual textured surface can yield evocative experiences [23], but fall short of perceptual realism and physical accuracy. The complex morphology, and highly viscoelastic nature of the finger makes it difficult to adapt existing models for tool-mediated texture rendering to direct finger contact, although the system identification methods we investigated here are inspired by such approaches.

In this study, building on our preliminary work [11], we developed a novel system for accurately capturing end-point forces felt by a finger sliding on a textured surface. We analyzed the extent of variation of these force signals in the temporal and spatial domains, and attempted to relate these to

The authors are with the Department of Electrical and Computer Engineering, Drexel University, Philadelphia, PA 19104 USA e-mail: marco.a.janko@drexel.edu.

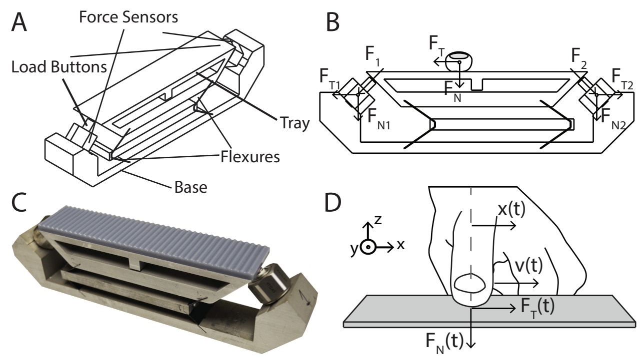

Fig. 1. **A** Isometric illustration of the apparatus. **B** Front view of the apparatus illustrating normal and tangential force decomposition during sliding contact with the finger. **C** Photo of the apparatus. **D** Relation between intrinsic surface geometry, fingertip position $x(t)$, scanning speed $v(t)$, and mechanical forces $F_N(t)$ and $F_T(t)$ exerted by the finger.

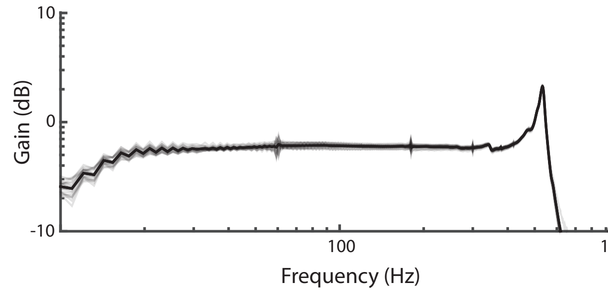

Fig. 2. Frequency Response Function (FRF) of the force sensing apparatus in the tangential direction. Twenty individual trials in gray, average in black. The FRF shows a resonant mode above 500 Hz and low amplitude interference from the power supply at 60 Hz and its harmonics. The usable bandwidth is approximately from 15 - 500 Hz.

the geometry of the surface and contact parameters, including sliding speed and contact force, with the aim of characterizing the relation between both. The resulting force signals proved remarkably unpredictable, reinforcing the challenge involved in haptic texture perception.

II. Methods

We created a system for capturing mechanical interactions and kinematics of a finger sliding on textured surfaces, which we fabricated to precise geometric specifications. The surfaces were sinusoidal gratings, with different wavelengths and amplitudes. We measured force and kinematic data as individuals explored these surfaces with their index fingers, at specified speeds and normal forces. In order to identify invariant properties of these interactions, we analyzed the force patterns in the spatial domain, and aligned them, compensating for fine variations in contact position from trial to trial. We used signal analysis and system identification methods to characterize the resulting force patterns and to quantify the possibility of predicting forces from texture geometry.

A. Measurement Apparatus

The apparatus included a novel force sensing instrument, an optical motion capture system, data acquisition hardware, and a personal computer running custom software, including a graphical user interface (GUI) that was used to monitor data collection and provide feedback during the experiments.

We designed and fabricated a custom sensing instrument (Fig. 1) to precisely capture forces applied by a finger sliding on a textured surface. The sensor consisted of a rigid tray suspended on a compliant mechanism. Two pairs of flexure hinges provide constraints that limit the motion in all but the horizontal and vertical directions. The device structure was designed using compliant mechanism theory [19], solid (CAD) modeling and simulated using finite element method numerical simulation (COMSOL Multiphysics, Boston, MA), ensuring a usable measurement bandwidth extending to 500 Hz. We fabricated the rigid sections of the device from type 6010 aluminum alloy using precise electrical discharge machining, and constructed the flexures from 0.25 mm type 1095 spring steel. The top section of the tray (top dimensions 120×25 mm) was specified to support textured surfaces that were to be used for the measurements.

Electronic sensing was performed by a pair of piezoelectric force sensors (Model 9712A5, Kistler Instruments, Winterthur, Switzerland) terminating on hemispherical contact buttons, and positioned to contact the tray at 45° angles (Fig. 1B), allowing normal and tangential force components to be measured. The sensors were powered using an Integrated Electronics Piezo Electric (IEPE) compliant supply (Model 5134, Kistler Instruments), and signals from each sensor were conditioned and digitized (55.6 us sample period, 16 bits) using data acquisition hardware (NI 9215 and Compact DAQ, National Instruments Inc., Austin, TX).

Due to the 45° orientation, the force signals F_1 and F_2 measured by the sensors are linear combinations (with equal weights) of the force components normal and tangential to the surface, F_N and F_T, of the resultant force applied to the tray

$$F_N = \frac{1}{\sqrt{2}}(F_1 + F_2), \qquad F_T = \frac{1}{\sqrt{2}}(F_1 - F_2) \tag{1}$$

An experimental frequency response function (FRF) was measured using a pendulum to strike the tray horizontally on a flat sample fabricated using the same material as the sinusoidal gratings. A total of 20 trials were measured and the frequency response was obtained by transforming the resulting force signals using the Fourier transform (Fig. 2). We calibrated the electronic sensor using a step force input of known magnitude, the electronic measurements required an amplification of 3.7 dB relative to the manufacturer's specifications.

Kinematic trajectories of the finger were captured using an optical motion capture system (V120:Trio Natural Point, Corvallis, OR). This system tracked a small reflective marker that was adhered to the fingernail in a standardized location. The optical motion capture system operated with a sampling period of 8.3 ms and an approximate spatial resolution of 0.2 mm. It was positioned and calibrated to have the zero reference at the center of the apparatus along the *x* axis (Fig. 3). Data acquisition and optical motion capture were managed

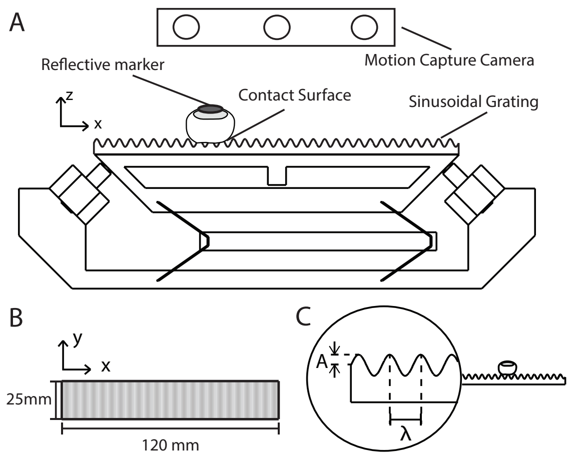

Fig. 3. **A** Experimental system designed to measure displacement, normal and tangential forces during sliding contact between a finger and a textured surface. Top (**B**) and front (**C**) view illustrations of one of the eight textured surfaces (all sinusoidal surfaces) used in the experiment; Top dimensions as shown. Eight different textures were employed, differing in a single parameter (spatial scale).

by a computer running a custom software GUI (MATLAB Release 2014b, The MathWorks, Inc., Natick, Massachusetts) that controlled the data recording process.

B. Textured Surfaces

We fabricated textured surfaces with known geometries, which were specified through height functions $h(x)$, in order to study the variation of forces with surface geometry during sliding touch of these surfaces with the finger. These surfaces were sinusoidal surfaces with height profiles given by $h(x) = A\sin(2\pi x/\lambda)$. Amplitude A and spatial wavelength λ varied for each sample. Eight such surfaces were used in the experiment, with λ = 0.5 mm, 1 mm, 1.5 mm, 2 mm, 2.5 mm, 3 mm, 3.5 mm and 4 mm (similar range to the stimuli used in previous studies of texture perception from resultant end point forces [12], [18]). The amplitude of each sinusoidal surface was equal to a fixed fraction of the wavelength for all samples, $A = 0.1\lambda$, ensuring that the maximum slope was constant for all sinusoidal surfaces – only the scale varied. We considered different surface geometries and amplitude-wavelength relations in this work, but elected to focus on a single effective parameter (scale), for practical reasons, and to aid the interpretation of the results. All surfaces were 120 mm long and 25mm wide (Fig. 3 B,C). The surfaces were modeled parametrically in software and fabricated using a photopolymer resin 3D printer (Objet 30, Stratasys Inc., Boston, USA) yielding an artifact-free finish at the scales of interest (approximate resolution: 100 μm). No further processing was performed to modify the surface finish. The surfaces were firmly affixed to the measurement apparatus with two-sided adhesive tape during the experiments.

C. Measurement Procedure

The measurement apparatus was used to capture normal forces, tangential forces, and movement during sliding contact of a bare finger on a textured surface. Nine individuals participated in this experiment (5 male and 4 female, ages 19 to 28). None evidenced any abnormality of biomechanics or function of the finger or hand, and all were right hand dominant. Each participant was seated in front of the apparatus with the right elbow supported and forearm held at a comfortable angle. They each performed sliding touch of the eight different sinusoidal surfaces a total of 30 times in alternating directions, using the second digit of the right hand. There were four different measurement conditions (Table. I), which varied in nominal scanning speed (80 mm/s and 120 mm/s) applied normal force (0.3 N and 1 N).

TABLE I. MEASUREMENT CONDITIONS FOR THE EXPERIMENT

	Conditions			
	C1	C2	C3	C4
Prescribed sliding speed v	80 mm/s	80 mm/s	120 mm/s	120 mm/s
Prescribed normal force f	0.3 N	1 N	0.3 N	1 N

In order to enable participants to produce normal forces and sliding speeds close to those that were specified during the experiment, feedback was provided during practice trials via an automated system. A graphical user interface indicated the force level to be produced relative to that performed by the participant during the trial. An audio metronome was used to enforce sliding speed, by indicating the regular tempo at which the finger was to be slid across the surface. Participants were readily able to follow the metronome, but there were variations in force and speed trajectories, due to normal human motor control limitations, as discussed below. Training was provided in advance of each of the four measurement conditions and continued until the participant achieved consistent performance as determined by the experimenter. Prior to data collection in each condition, each of the sinusoidal gratings and finger pad were cleaned using a cotton cloth and isopropyl alcohol.

D. Data Processing

The discrete time signals from each force sensor were digitized, and used to compute normal and tangential force components $F_N(t)$ and $F_T(t)$ (Eq. 1). The measurement conditions were indexed by the surface texture wavelength λ, and the prescribed force level f and prescribed speed v. We also recorded the position $p(t)$ of the finger, but only the x-component was employed. Subsequent processing stages are summarized in Fig. 4. The force signals were band pass filtered to remove effects of motor variability and high frequency artifacts. This was accomplished with a zero-phase filter with cutoff frequencies of 15 and 500 Hz. Three zero-phase notch filters (60 Hz, 180 Hz and 300 Hz) were used to eliminate a small amount of power supply interference (Fig. 2); the narrow bandwidth and linear phase response ensured the filter could correct for this interference without significantly affecting the measurements. Position information was re-sampled to 18 kHz to match the sampling frequency of the force data.

Further analysis focused on the tangential (frictional) force component $F_T(t)$. We segmented these signals into trials, each of which consisted of one left-to-right scan of the middle 80 mm of the respective surface. We eliminated 20 mm at

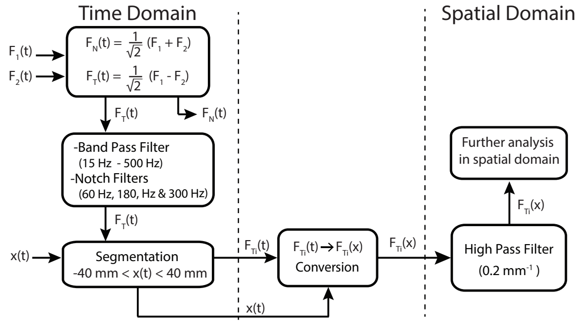

Fig. 4. Signal processing of the measurements captured in the present investigation, including both time and space domain processing.

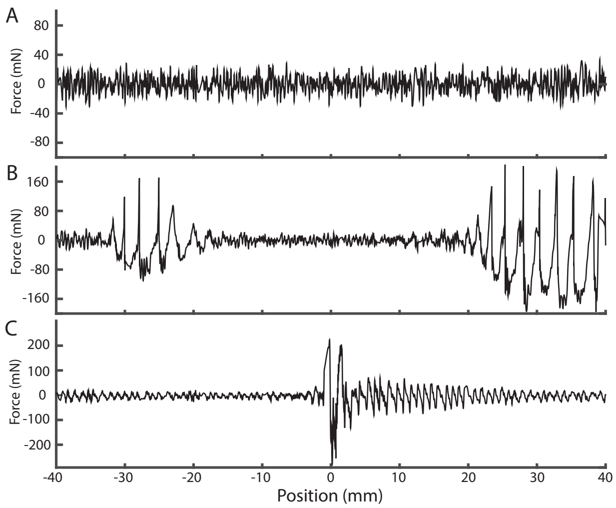

Fig. 5. Example tangential force signals with and without stick-slip. **A** Trial without stick-slip events, $\lambda = 0.5$ mm, prescribed speed $v = 80$ mm/s, prescribed normal force $f = 1$ N. **B** Trial exhibiting stick-slip oscillations, $\lambda = 0.5$ mm, $v = 80$ mm/s, $f = 1$ N. **C** Trial exhibiting transient stick-slip events, $\lambda = 0.5$ mm, $v = 80$ mm/s, $f = 1$ N.

each end of the trial to avoid transient effects accompanying the change in direction of motion. For each of the eight wavelengths, two force levels, and two speeds, we considered ten left-to-right trials from each of the nine participants, yielding a total of 2880 signals that were used for our analysis.

Using the method of Wiertlewski et al. [32], we transformed the tangential force for each trial from the time to the spatial domain, yielding a spatial force pattern $F_T(x)$ given by

$$F_T(x) = \mathcal{F}_T((\mathcal{X}^{-1}(x)) \tag{2}$$

Here, $\mathcal{F}_T(t)$ and $\mathcal{X}(t)$ are piecewise linear approximations to $F(t)$ and $x(t)$. The inverse function of $\mathcal{X}(t)$ was resampled at regular distances, yielding a spatial sample period of 0.01 mm. The resulting spatial domain tangential force data were filtered using a zero-phase high-pass filter with cut-off frequency at 0.2 mm^{-1} to eliminate slow varying fluctuations in the data.

E. Stick Slip Phenomena

A small number of trials in each condition (fewer than three for every participant) exhibited periodic or transient frictional stick slip events, marked by a sustained increase of force magnitude followed by a rapid decrease in force (Fig. 5). Consistent with expectations from basic mechanics, these could be assumed to reflect the occurrence of static finger-surface contact (sticking), followed by the rapid resumption of sliding motion (slip) [2], [20], [25]. Although interesting, these events occurred sparsely and at irregular intervals, and were larger in force magnitude than the regular variations in texture-produced forces that we observed. Consequently, we removed trials in which stick slip events were identified, eliminating a number between 0 and 2 trials for each participant and condition (0 being the common case).

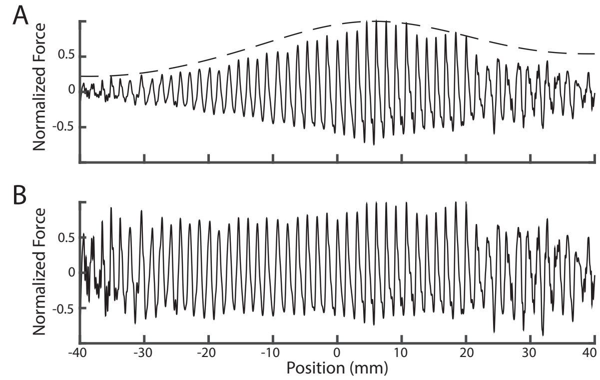

Fig. 6. Example trial, $\lambda = 1.5$ mm, prescribed speed $v = 120$ mm/s, prescribed normal force $f = 0.3$ N. **A** Before amplitude demodulation. Force $\tilde{F}_T(x)$ in black, envelope $F_E(x)$ in dashed lines. **B** Demodulated force pattern, $F_T(x)$.

F. Amplitude Demodulation

In order to eliminate effects of amplitude modulation in the force signals, which were due to changes in the average normal force applied caused by variations in motor activity during sliding of the finger, we processed the force signals in order to remove the modulating effects of an envelope signal $F_E(x)$ using a square law envelope detector, given by

$$\tilde{F}_T(x) = F_T(x)F_E(x), \tag{3}$$

$$F_E(x) = \sqrt{F_T(x)^2 * h_{LPF}(x)} \tag{4}$$

Here $h_{LPF}(x)$ is a zero-phase low-pass filter (cutoff freq. 0.05 mm^{-1}), and $*$ denotes convolution. For each trial, we divided the force signal by the envelope estimate, and normalized the resulting signal (peak amplitude 1 mN), see Fig. 6.

G. Optimal Phase Alignment

In order to facilitate the analysis of trial to trial variations in force signals, we processed the force data to compensate for fine differences in contact position between the finger and the surface, which could be attributed to finger orientation or mechanical factors, using an optimization based phase alignment method, and performed an inter-session alignment in order to eliminate phase artifacts due to small variations in

$\overline{C} \leftarrow -1$
$\overline{F}_T(x) \leftarrow \frac{1}{n}\sum_{i=1}^{n} F_{T,i}(x)$
$\overline{C}' \leftarrow \frac{1}{n}\sum_{i=1}^{n} \rho(F_{T,i}(x), \overline{F}_T(x))$
while $(\overline{C} < 1.05\,\overline{C}')$ **do**
  for $i = 1$ **to** n **do**
    $\tau_i \leftarrow \arg\max_{\tau}\ \rho(F_{T,i}(x-\tau), \overline{F}_T(x))$
  end for
  $\overline{F}_T(x) \leftarrow \frac{1}{n}\sum_{i=1}^{n} F_{T,i}(x-\tau_i)$
  $\overline{C} \leftarrow \overline{C}'$
  $\overline{C}' \leftarrow \frac{1}{n}\sum_{i=1}^{n} \rho(F_{T,i}(x-\tau_i), \overline{F}_T(x))$
end while

Fig. 7. Trial alignment algorithm; The quantities $\overline{C}$ and $\overline{F}_T$ were computed on the middle 60 mm of each trial.

system calibration between measurement sessions. The technique we used was inspired by methods previously developed for image comparison in computer vision [14]. The essence of the approach is to determine a rigid displacement τ (in mm) for every trial such that the difference between the force patterns in the ensemble of trials is minimized. To this end, we first aligned all trials in each condition (λ, v, f) for each participant, in order to compensate for contact mechanical variations due to participant motor behavior. We then estimated a constant phase shift between participants, in order to compensate for artifacts of the measurement configuration (i.e., slight differences in the position of the optical marker and surface position).

To align trials, we used an optimization algorithm (Fig. 7) similar to expectation-maximization, which alternately computed the mean force pattern $\overline{F}_T(x)$ for a given set of offset values τ_i (i indexes the measurement trial)

$$\overline{F}_T(x) = \frac{1}{n}\sum_{i=1}^{n} F_{T,i}(x+\tau_i)$$

and selected the displacements τ_i that maximized, in the respective condition, the (normalized) resultant correlation coefficient $\overline{C}$ with the mean force pattern $\overline{F}_T(x)$,

$$\rho(X,Y) = \frac{E(XY)-E(X)E(Y)}{\sqrt{E(X^2)-E(X)^2}\sqrt{E(Y^2)-E(Y)^2}} \quad (5)$$

$$\overline{C} = \frac{1}{n}\sum_{i=1}^{n} \rho(F_{T,i}(x+\tau_i), \overline{F}_T) \quad (6)$$

Here $\rho(X,Y)$ is Pearson's correlation coefficient. These two steps were iterated until convergence. The value $\overline{C}$ employed here is similar to the r^2 value for a regression fit. τ_i was constrained to the range from -2 to 2 mm, and the minimum permissible change in displacement was 10 μm. The algorithm terminated when $\overline{C}$ increased by less than 5% (Fig. 7).

H. Signal Entropy

Inspired by prior literature on image alignment [10], [14], we used entropy as an independent assessment of the quality of the phase alignment of the force signals, by computing its change, in each condition (λ, v, f), before and after alignment. Entropy provides a nonparametric measure of the degree of disorder or dispersion in a distribution of values. Denote by $D_{\lambda,v,f}(F)(x)$ the empirical distribution (histogram) among all trials of force values at position x in condition (λ, v, f). The empirical entropy of the ensemble of N signal values at x is given by

$$H_{\lambda,v,f}(x) = -\sum_j D(F_T(x))_j \log_2 D(F_T(x))_j \quad (7)$$

where $D(F_T(x))_j$ is the number of values of $F_T(x)$ in the jth histogram bin. We computed the total entropy among all trials in each condition by integrating the pointwise empirical entropy over the sample

$$\overline{H}_{\lambda,v,f} = \int H_{\lambda,v,f}(x)\,dx \quad (8)$$

The change in entropy after alignment provided a measure of the extent to which the rigid translations τ_i resulting from the alignment procedure reduced trial to trial variability in the force signals. Stated differently, the entropy values quantified how well the observed variability in force signals could be accounted for by small trial to trial changes in contact position.

I. Signal Variance

In order to compare the extent of variation in force signals F_T across trials in each condition (λ, v, f), we computed the ratio of the average signal variance to the RMS amplitude of the mean force pattern $\overline{F}_T(x)$. This ratio, which we refer to as Variance-to-Power Ratio (VPR), is given by

$$\mathrm{VPR} = 100\left(\frac{\frac{1}{n}\sum_{i=1}^{n}\mathrm{var}(F_T(x))}{\mathrm{rms}(\overline{F}_T(x))}\right), \quad (9)$$

$$\mathrm{rms}(X) = \sqrt{\frac{1}{N}\sum_{n=1}^{N}|X_n|^2}. \quad (10)$$

This ratio was higher when the signal mean in a given condition was less representative of the individual trial measurements.

J. Nonlinear Distortion

Forces produced as a result of mechanical interactions associated with sliding contact of a finger against a textured surface can exhibit significant nonlinearities [1], [31]. The sinusoidal excitation of a nonlinear dynamical system can yield harmonic signal distortion, which is reflected in the total harmonic distortion (THD) of the input-output response of the system given by

$$\mathrm{THD} = \frac{\mathrm{rms}(F_T - H_0)}{\mathrm{rms}(H_0)} \quad (11)$$

We computed THD in each condition (λ, v, f) in order to quantify the extent to which our measurements may have reflected such nonlinearities. We extracted the first harmonic component of the signal H_0 (which coincided with the spatial frequency of the surface) using a band pass filter with a narrow bandwidth of 0.04 mm^{-1} about the fundamental frequency.

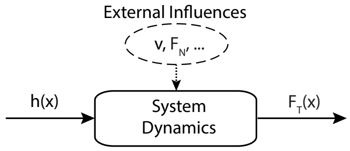

Fig. 8. Nonlinear dynamical system model mapping an input geometry $h(x)$ to output force pattern $F_T(t)$. Parameters include the speed v, contact force f. It could be assumed to depend on other factors such as temperature and humidity.

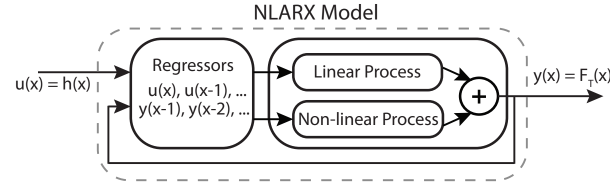

Fig. 9. Block diagram of the Non Linear Auto-Regressive eXogeneous (NLARX) model.

K. Predictive Modeling

We measured force signals produced by interactions between the finger and the textured surface. In order to shed light on these interactions, we adopted an input-output system model with the surface texture height function $h(x)$ as the input and the friction force $F_T(x)$ as output (Fig. 8). Other parameters affecting the interaction (sliding speed, normal force, humidity, etc.) were regarded as constant (the foregoing processing helped to ensure this). We adopted a deterministic model, since the fundamental physical processes involved are not stochastic at the length scales of interest, and utilized nonlinear models, since such interactions are known to possess nonlinearities (as further supported by the outcome of the foregoing analysis; See Results, below).

To model our data, we adopted a general black box nonlinear system modeling approach, utilizing Nonlinear Auto Regressive Exogenous (NLARX) Models (Fig. 9). We trained these models on a subset of our data, and assessed their ability to predict forces from surface texture using an independent data set as a control.

The NLARX model related an input signal $u(x) = h(x)$ to an output $y(x) = F_T(x)$ via a time delay nonlinear autoregression. The vector of regressors $\mathbf{r}(x)$ at each x was given by

$$\begin{aligned} \mathbf{r}(x) &= (u(x)\ u(x-\delta)\ \cdots\ u(x-(n_i-1)\delta) \\ &\quad y(x-\delta)\ \cdots\ y(x-n_o\delta))^T \end{aligned} \tag{12}$$

where $\delta = 0.01$ mm is the spatial sampling interval. The output $y = y_{\text{lin}} + y_{\text{nl}}$ was a sum of linear and nonlinear terms (Fig. 9), with a linear part given by

$$y_{\text{lin}}(x) = \mathbf{a}^T \mathbf{r}(x) \tag{13}$$

where $\mathbf{a}$ is a vector of linear regression weights that were estimated from data. The nonlinear component had the form of a wavelet nonlinearity

$$y_{\text{nl}}(x) = \sum_{i=1}^{n_w} \alpha_i \kappa(\beta_i(\mathbf{r}(x) - \bar{\mathbf{r}} - \mathbf{c}_i)), \tag{14}$$

$$\kappa(\mathbf{u}) = (N - \|\mathbf{u}\|^2) e^{-0.5\|\mathbf{u}\|^2} \tag{15}$$

The parameters α_i, β_i and $\mathbf{c}_i$ were the wavelet coefficient, dilation, and translation parameters that were estimated from data as part of the regression. The number of parameters and model order were determined by values (Table II-K) obtained via model selection (see below). Estimation was performed with Levenberg-Marquardt search, using the Matlab system identification toolbox (Matlab Release 2014b, The MathWorks, Inc., Natick, Massachusetts).

The NLARX model structure was selected because it provided a higher average goodness of fit (GOF) metric (on the data subset tested) than that of several other model alternatives that we evaluated, which included Hammerstein-Weiner (with static nonlinearity) models and linear autoregressive models. The nonlinear part of the NLARX model used was chosen to be modeled by a wavelet network. This type of nonlinearity was selected because its use resulted in a higher average GOF (on the data subset tested) than that of other evaluated alternatives, including single and multiple layer sigmoidal neural networks

The regression weights $(a, m, \alpha_i, \beta_i, \mathbf{c}_i)$ were estimated to minimize the RMS error $\epsilon(y, \hat{y}))$ between the measurements $y(x)$ and the model output $\hat{y}(x)$, where

$$\epsilon(y, \hat{y}) = \frac{\|y - \hat{y}\|}{\|y - \bar{\hat{y}}\|}, \qquad \bar{\hat{y}} = \frac{1}{n} \sum_{x=1}^{n} \hat{y}\ . \tag{16}$$

We estimated an NLARX model for each trial in the spatial domain (60 mm in length), using the first 40 mm for model estimation, and the second 20 mm for testing. Our test criterion was the GOF metric

$$\text{GOF} = 1 - \epsilon(y, \hat{y}) \tag{17}$$

Before training and testing, we used a model selection procedure to determine the order parameters n_i, n_o, n_k and n_w best suited to each measurement condition (Table II-K). In order to avoid overfitting, we used independent data sets for this purpose, consisting of ten randomly selected trials in each measurement condition; these trials were subsequently excluded from training and testing. A grid search over all even values of the model order parameters was used in order to select those that maximized the sum of GOF metrics between the trials in each respective condition (Table II-K).

TABLE II. NLARX MODEL PARAMETERS AND SEARCH RANGE

Parameter	Description	Span
n_i = 2k	Num. Input regressors	k = 1,2,3, ... ,15
n_o = 2k	Num. Output regressors	k = 0,1,2, .. . ,15
n_w = 5k + 1	Num. Wavelets	k = 0,1,2,3,4,5,6,7
n_k = 4k	Num. Nonlinear regressors	k = 0,1,2,3,4,5

III. Results

A. Force Patterns Before and After Phase Alignment

The ensemble of trials in each condition exhibit significant variation about the mean $\overline{F}_T(x)$ (Fig. 10) both before and after

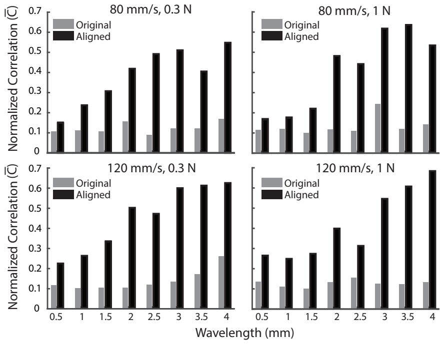

Fig. 11. Normalized correlation $\overline{C}$ vs. sinusoidal surface wavelength under four measurements conditions, before and after alignment. The alignment process increases considerably the normalized correlation in all cases.

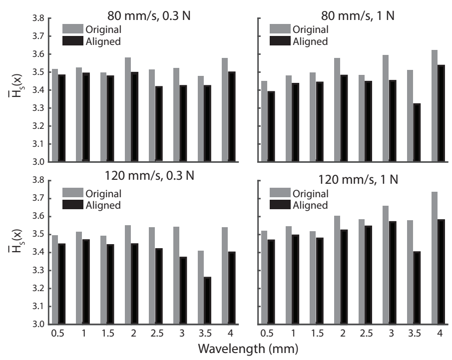

Fig. 12. Empirical entropy $\overline{H}_S$ vs. wavelength λ in all four conditions v, f. After the alignment process, the signals show a reduction in the average spatial entropy, indicating a reduction in the variability between trials.

phase alignment of trials. However, the amplitude of the mean signal was increased in all conditions. After alignment, the value of the normalized correlation coefficient $\overline{C}$ increased in all conditions (λ, v, f), and increased by more than 100% in 29 out of 32 conditions (Fig. 11). We used entropy values $\overline{H}_{\lambda,v,f}$ as an independent and nonparametric measure of the spread between trials. In all 32 conditions, the value of $\overline{H}$ decreased after alignment, indicating that entropy was reduced (Fig. 12).

The distribution of displacements τ that were obtained through the optimal alignment procedure provide an indication of the extent of variability in the effective phase offset between force patterns from trial to trial (Fig. 13,14). Although phase aligning the force signals greatly increased the correlation between trials and decreased the entropy, the values of τ needed to achieve this were very small, on the order of 0.1 mm. No qualitative differences were observed between conditions, and the distribution of displacements was also qualitatively similar for different subjects (Fig. 14).

B. Force Patterns in Spatial Domain

At all but the shortest wavelength λ, the mean force signals $\overline{F}_T(x)$ exhibit quasiperiodicity in all conditions, with the wavelength of force oscillation equal to that of the surface (Fig. 10). Individual trials also exhibited irregular quasiperiodicity (e.g., Fig. 8). We further measured the extent of variance

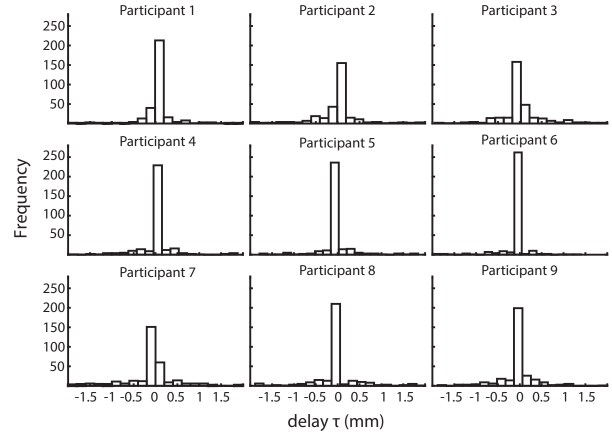

Fig. 13. Phase alignment histogram grouped by participant. Typical values of τ were small, approximately 0.1 mm.

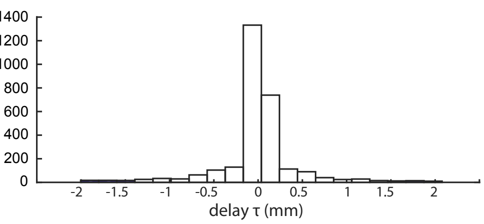

Fig. 14. Phase alignment histogram for all participants.

about the mean signal in each condition using a variance-to-power ratio (VPR, Fig. 16). In all conditions, the highest two values occurred at the shortest wavelength, and the lowest value occurred at one of the longest wavelengths, indicating that there was more variance about $\overline{F}_T(x)$ at low wavelengths, and that the mean $\overline{F}_T(x)$ was more representative at long wavelengths. The data analysis in the spatial frequency domain provided evidence of nonlinearities, in the form of frequency content that was harmonically related to the periodicity of the surface texture (Fig. 15). The nonlinearity of the finger-surface interactions is evidenced by the multiple harmonics that are present in the force data. Consistent with prior literature [11], [31], the harmonic amplitude decreased with increasing harmonic number.

Total harmonic distortion (THD) was used to measure nonlinearity in the source interactions (Fig. 17). These values decreased with wavelength for all values of (v, f), indicating an increasingly nonlinear relationship between force and surface geometry at smaller spatial scales, or shorter wavelengths.

C. Predictive Modeling

We assessed the extent to which force patterns $F_{T,i}(x)$ could be predicted from surface height $h(x)$ using Nonlinear Autoregressive Exogenous (NLARX) modeling. The prediction quality on the test set is shown for all conditions (λ, v, f) in Fig. 18. A separate model was fit for each trial, and the model structure was constant for all trials in a given condition (λ, v, f). We assessed fit quality by computing the average

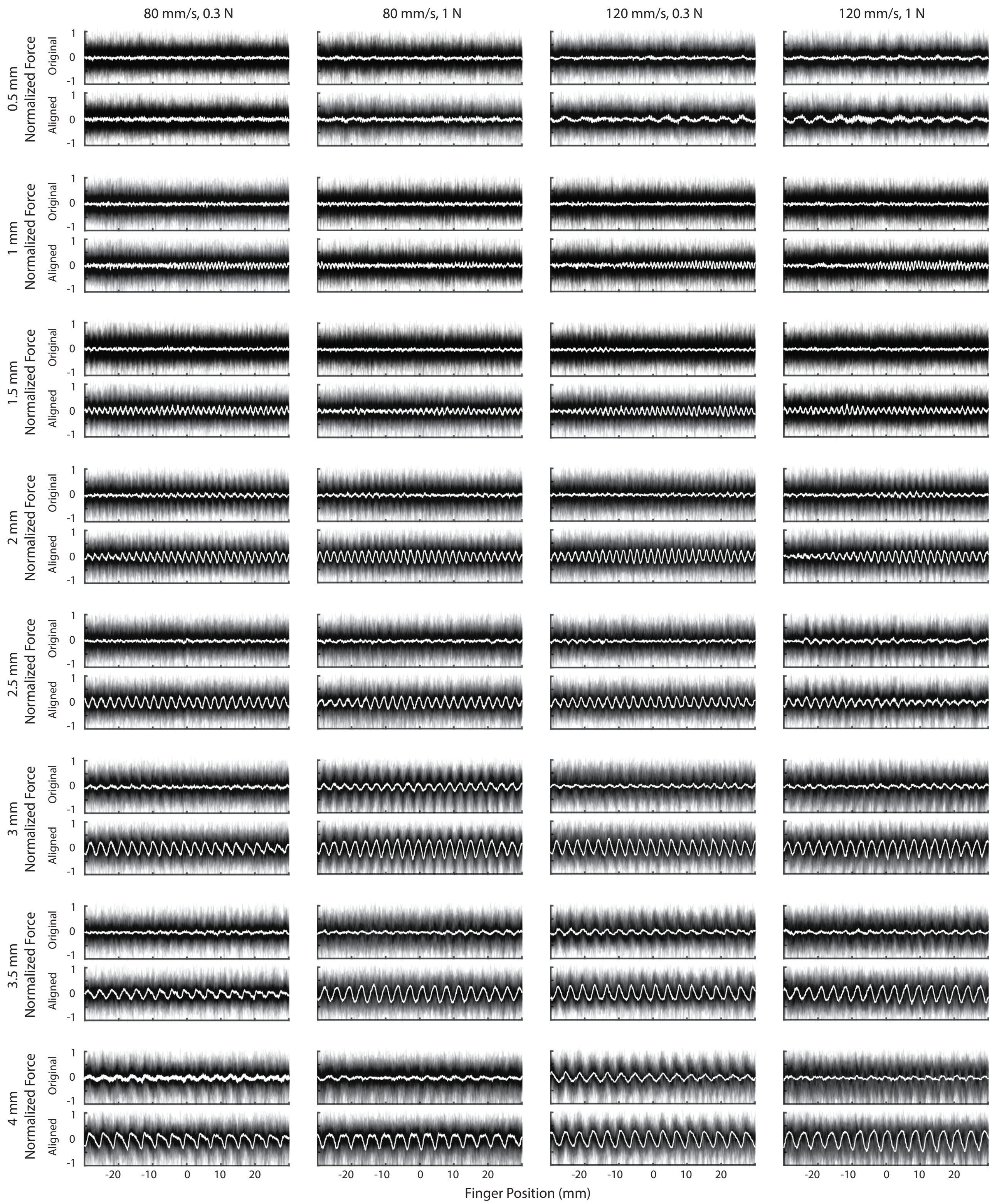

Fig. 10. Illustration of the effect of alignment under the 32 measurement cases (2 forces f, 2 speeds v and 8 wavelengths λ). Trials corresponding to all subjects, single trials $F_T(x)$ in black, trials average $\overline{F}_T(x)$ in white. The average between all trials with $\lambda > 1$ mm, shows a pseudo-periodic behavior with the same wavelength as the sinusoidal surface used. The patterns in the averages for the $\lambda = 0.5$ mm and 1 mm surfaces are less readily distinguished by inspection.

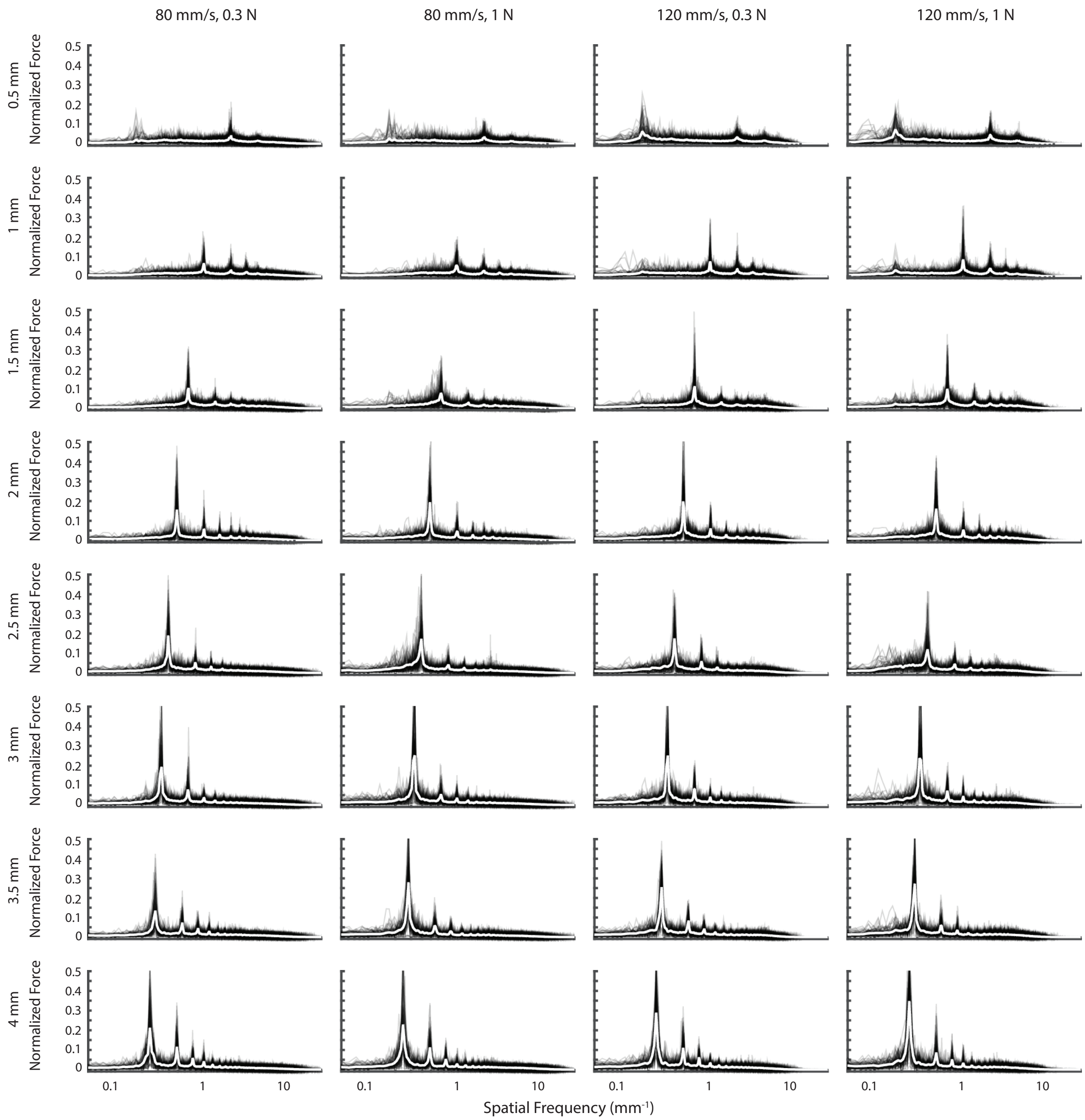

Fig. 15. The spatial magnitude spectrum of force patterns in all recorded trials (black lines), and all measurement conditions (λ, v, f). Average of spatial magnitude spectra in white. A series of decaying harmonics is evident, dominated by a fundamental frequency component with the same spatial frequency as the surface texture. Harmonic content for the high spatial frequency surfaces was less evident. In addition, these surfaces manifested a low frequency peak that may be attributed to finger pad mechanics or to low frequency surface noise (which was high-pass filtered in pre-processing stages) or other factors.

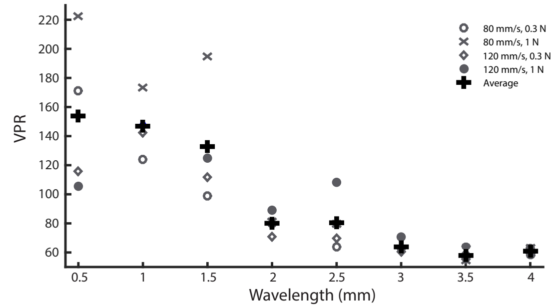

Fig. 16. Average of Variance-to-Power Ratio (VPR) computed in 90 trials per each wavelength and experimental conditions (λ, v, f). Different experimental conditions in gray markers, the average VPR of the VPR under the four conditions is shown as black crosses.

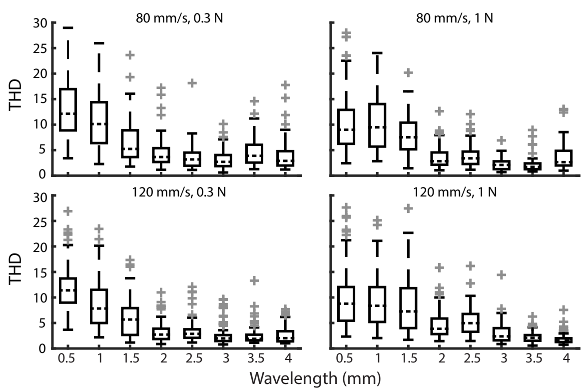

Fig. 17. Average of Total Harmonic Distortion (THD) computed in 90 trials per each wavelength and experimental conditions (λ, v, f). Each box plot delimits the region where 80 % of the samples lie, median values marked as dashed lines, outliers marked as gray crosses (Some data points are outside the plot area).

GOF metric for each trial on a moving 4 mm prediction window (Fig. 18). The GOF metric could be positive or negative, with higher (more positive) values indicating a better fit. The results increase from near zero at small wavelengths to values of approximately 10, indicating relatively poor predictability in all conditions, but especially so at small spatial wavelengths.

We further investigated the predictability of force patterns from surface geometry by computing correlation values between the model predictions and measurements on a 4 mm prediction horizon, by averaging values of Pearson's correlation coefficient between trials (Fig. 19). The highest mean correlation values, near $\overline{\rho} = 0.5$, were observed at the longest wavelengths, indicating that model predictions best matched measurements for the most slowly varying surfaces, but also reinforcing the observation that the force data exhibited important variations, even within a single trial.

IV. Discussion

The results provide concrete insight into the frictional forces that are produced during bare finger sliding contact, and their relation to the geometry of the underlying surface, as well as interaction parameters (v, f). Most notably, the data we captured exhibited large variability between trials, in essentially

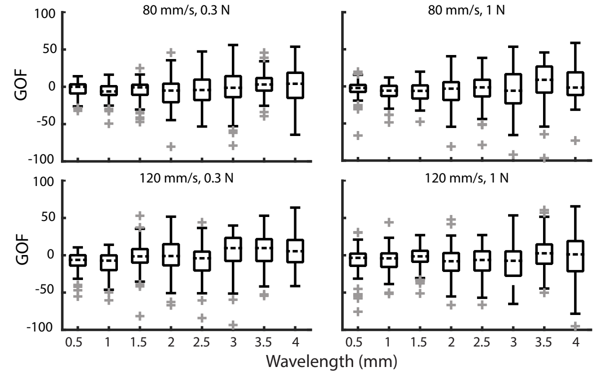

Fig. 18. Average of NLARX prediction GOF at 4 mm prediction window computed in 90 trials per each wavelength and experimental conditions (λ, v, f). Each box plot delimits the region where 80 % of the samples lie, median values marked as dashed lines, outliers marked as gray crosses (Some data points are outside the plot area).

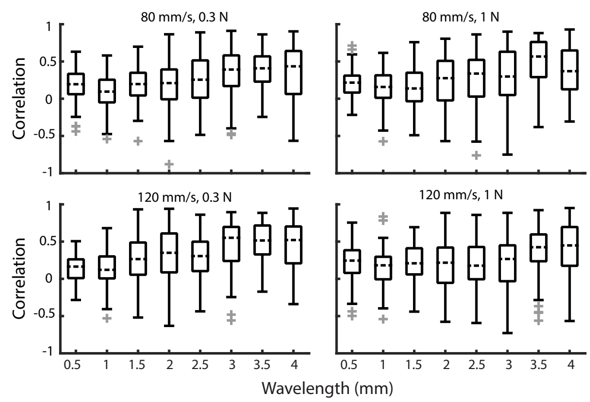

Fig. 19. Average of NLARX prediction correlation at a 4 mm prediction window computed in 90 trials per each wavelength and experimental conditions (λ, v, f). Each box plot delimits the region where 80 % of the samples lie, median values marked as dashed lines, outliers marked as gray crosses (Some data points are outside the plot area).

all conditions. We hypothesize that this variability is due, in part, to small trial to trial variations in contact conditions. Indeed, our results show that by introducing small signal-dependent offsets in displacement, which were determined through optimization to be on the order of 100 μm, it was possible to greatly increase the amplitude of the mean force pattern in every condition (λ, v, f), and to reduce the empirical entropy of the force signal ensemble.

Our analysis methods, including spatial domain processing and amplitude demodulation, expressly compensated for variations in applied force f and speed v. Nonetheless, it is also possible that small trial-to-trial variations in applied force and speed contributed to the trial-to-trial variations in force that were observed. A further cause may be the nonlinear dynamical nature of the interactions themselves, which can exacerbate all of the aforementioned effects, since nonlinearity is known to amplify dynamical sensitivity to initial conditions. Our analysis demonstrated that at least one measurement of nonlinearity, THD, was highest for textures with the smallest wavelengths. The presence of such nonlinearities was consistent with predictions from prior literature [32]. These same textures exhibited the highest Variance-to-Power Ratio (in all conditions (v, f)), indicating that highest trial-to-trial variability where interactions were found to be most nonlinear. Nonetheless, the analysis revealed that several signal features, including the fundamental frequency of spatial force patterns, were stable and well preserved, especially for $\lambda > 1$ mm, despite these variations. Such signal components might be hypothesized to be cues that aid the perceptual recovery of surface texture. For smaller wavelengths ($\lambda = 0.5, 1$ mm), however, the fundamental and harmonic components of the signals were less prominent.

Although we evaluated a large number (nearly 8000) candidate models for predicting spatial force patterns $F_T(x)$ from surface height $h(x)$, the NLARX system models we estimated from data proved to have limited predictive power, even when evaluated on a short horizon of 4 mm, possibly due to the aforementioned signal variability. Consequently, it was difficult to identify any clear relation between the interaction conditions and the quality of fit (GOF metric) or the correlation between the true and predicted force pattern. However, we did observe modestly higher correlation values in the long wavelength conditions, which might indicate that prediction is somewhat more accurate at longer spatial scales. In previous work (using data captured from a different apparatus and different textured surfaces), we observed that it was possible to predict the mean force pattern $\overline{F}_T(x)$ with reasonable quality using similar models, and that prediction quality was dramatically better at wavelengths λ of at least 3 mm [11]. However, perhaps due to the overwhelming variability in the force signals recorded in individual trials, as were analyzed in the present experiment, no clear conclusion could be drawn here about the predictability of forces produced from interaction with long versus short wavelength surface textures.

V. Conclusion

The forces that result from sliding contact of a bare finger with a textured surface depend on a number of factors, including the geometry of the surface, the detailed nature of finger-surface contact, and the time-varying exploratory trajectory of the finger. Here we focused on the integrated (resultant) frictional force between the finger and surface. Our results suggest that macroscopic knowledge of these parameters is insufficient to constrain force production. Even when sliding over very regular textures, and correcting for temporal and contact differences, frictional forces were observed to vary greatly from moment to moment and trial to trial.

Although our study did not directly investigate texture perception, it does raise relevant questions. Informally, the textured surfaces used in this investigation all feel highly regular; when exploring them with the finger one is left with the impression of a perceptually constant, regular, corrugated surface. This stands in stark contrast to the variability seen in individual force trials, from which one might, a priori, expect a perceiver to feel something different every time that the finger is stroked along the sample. How is the apparent perceptual stability of surface texture achieved, and which features of these signals enable the nervous system to solve this problem? The latter question is also highly relevant to the problem of haptic rendering. Many techniques have been developed for accurately reproducing frictional forces produced by a virtual surface, including those based on force feedback devices [4] and surface haptic displays [34]. Although other possibilities have been explored in the literature, one attractive option is to specify the surface texture geometrically, in the spatial domain. However, our results strongly suggest that such a specification, even when combined with measured interaction parameters (such as speed, position, and normal force), are by themselves insufficient to constrain the actual forces that should be produced in order to simulate interactions with the surface. Consequently, it is far from clear what rendering algorithm might be appropriate for producing realistic texture-generated forces from geometric surface specifications. One approach to this problem could be based on perceptual criteria, but as alluded to above, it is not obvious what the most perceptually salient features of these force signals may be.

Despite the promising nature of this study, several open questions remain, and additional research could shed further light on them. Based on our experiment, it was not possible to definitively identify the origin of the force fluctuations that we observed. Possible factors include the continuum dynamics of the finger pad, interactions with the finger ridges, the multi-contact surface that is involved, the presence of unstable stick-slip motion, or other unstable or chaotic modes of oscillation (possibly created by nonlinearities in the finger-surface interaction forces). In order to clarify which of these may be important, further research is needed on the dynamics of force production between the bare finger and a textured surface. Although the measurement apparatus presented here improves greatly on that presented in our preliminary work [11], one with greater temporal resolution and bandwidth would further aid this line of inquiry. A system that facilitates direct measurement of the complex contact geometry and local forces would allow a more direct investigation of the mechanics involved, but such a device has not yet been realized. The nonlinear models that we developed, after extensive search in model space, used data driven system identification methods that proved unable to fully capture the dynamics of finger-surface interactions. While this suggests the challenging nature of this task, further work is needed in order to explore what model structures might more effectively capture the dynamics. In future efforts, we aim to develop force production models that explicitly integrate models of contact mechanics and finger dynamics. This work will also be complemented by research aimed at identifying the mechanical signal features that are most salient to texture perception. Finally, we studied force production for a limited range of surfaces, materials, and interaction parameters. We plan to generalize further in future work using periodic and non-periodic textured surfaces with different shapes and study the frictional forces elicited to better understand the how the texture profile and the finger account for their generation.

Acknowledgment

This work was supported by NSF award CNS-1446752.

Marco Janko received the M.S. degree in Electrical Engineering from Drexel University in 2013 and the B.S. degree in Electrical and Telecommunications Engineering from Universidad ORT, Uruguay in 2009. Mr. Janko is a PhD candidate in ECE at Drexel University, with the RE Touch Lab, studying touch-produced forces for haptic texture and shape synthesis. He serves as chair of the IEEE SIGHT group "Education Through Communication" conducting the project Teaching with Tablets in diverse countries.

Richard Primerano received combined B.S. and M.S. degrees in Electrical Engineering and the Ph.D. from Drexel University, in 2005 and 2010, respectively. In 2010, he joined Drexel University as an Assistant Professor in the College of Engineering. His professional interests include robotics, ultrasonic data communication, and RF communication systems. He is currently senior engineering staff at Lockheed Martin Advanced Technologies Lab.

Yon Visell is Assistant Professor, University of California, Santa Barbara, where he directs the NSF supported RE Touch Lab. Assistant Professor (2012-2015) in the ECE Department at Drexel University. Post-Doctoral Fellow (2011-2012) at the Inst. of Intelligent Systems and Robotics, Université Pierre et Marie Curie. PhD in Electrical and Computer Engineering from McGill University (2011). MA and BA degrees in Physics (Univ. Texas-Austin, Wesleyan Univ.). He spent over 6 years in industrial R&D for sonar, speech recognition, and music DSP.

REFERENCES

[1] F. Al-Bender and J. Swevers. Characterization of friction force dynamics. *Control Systems, IEEE*, 28(6):64–81, Dec 2008.

[2] O. M. Braun. Stick-slip vs. smooth sliding in the multicontact interface. *EPL (Europhysics Letters)*, 109(4), 2015.

[3] T. Callier, H. P. Saal, E. C. Davis-Berg, and S. J. Bensmaia. Kinematics of unconstrained tactile texture exploration. 113(7), 2015.

[4] Gianni Campion and Vincent Hayward. Fast calibration of haptic texture synthesis algorithms. *IEEE Transactions on Haptics*, 2(2), 2009.

[5] Pierre-Henri Cornuault, Luc Carpentier, Marie-Ange Bueno, Jean-Marc Cote, and Guy Monteil. Influence of physico-chemical, mechanical and morphological fingerpad properties on the frictional distinction of sticky/slippery surfaces. *Journal of The Royal Society Interface*, 12(110):20150495, 2015.

[6] Benoit Delhaye, Philippe Lefèvre, and Jean-Louis Thonnard. Dynamics of fingertip contact during the onset of tangential slip. *Journal of The Royal Society Interface*, 11(100):20140698, 2014.

[7] K. Drewing, A. Lezkan, and S. Ludwig. Texture discrimination in active touch: Effects of the extension of the exploration and their exploitation. In *Proc. IEEE World Haptics Conference*, pages 215–220, June 2011.

[8] Ramona Fagiani, Francesco Massi, Eric Chatelet, Yves Berthier, and Adnan Akay. Tactile perception by friction induced vibrations. *Tribology International*, 44(10):1100–1110, 2011.

[9] Ramona Fagiani, Francesco Massi, Eric Chatelet, Jean Philippe Costes, and Yves Berthier. Contact of a finger on rigid surfaces and textiles: friction coefficient and induced vibrations. *Tribology Letters*, 48(2):145–158, 2012.

[10] Gary B Huang, Vidit Jain, and Erik Learned-Miller. Unsupervised joint alignment of complex images. In *Computer Vision, 2007. ICCV 2007. IEEE 11th International Conference on*. IEEE, 2007.

[11] Marco Janko, Richard Primerano, and Yon Visell. Scale dependence of force patterns during the scanning of a surface by a bare finger. In *Haptics: Neuroscience, Devices, Modeling, Applications*. Springer, 2014.

[12] R.L. Klatzky and S.J. Lederman. Tactile roughness perception with a rigid link interposed between skin and surface. *Perception and Psychophysics*, 61(4):591–607, 1999.

[13] M.A. Lawrence, R. Kitada, R.L. Klatzky, and S.J. Lederman. Haptic roughness perception of linear gratings via bare finger or rigid probe. *Perception*, 36(4):547 – 557, 2007.

[14] E.G. Learned-Miller. Data driven image models through continuous joint alignment. *Pattern Analysis and Machine Intelligence, IEEE Transactions on*, 28(2), Feb 2006.

[15] Susan J Lederman. Tactile roughness of grooved surfaces: The touching process and effects of macro-and microsurface structure. *Perception & Psychophysics*, 16(2), 1974.

[16] Susan J Lederman. Tactual roughness perception: Spatial and temporal determinants. *Canadian Journal of Psychology/Revue canadienne de psychologie*, 37(4), 1983.

[17] Susan J. Lederman and Roberta L. Klatzky. Extracting object properties through haptic exploration. *Acta Psychologica*, 84(1):29 – 40, 1993. Tactile Pattern Recognition.

[18] Susan J Lederman and Roberta L Klatzky. Designing haptic interfaces for teleoperational and virtual environments: Should spatially distributed forces be displayed to the fingertip? In *Proceedings of the ASME Dynamic Systems and Control Division*, pages 11–15. American Society of Mechanical Engineers, 1997.

[19] Nicolae Lobontiu. *Compliant mechanisms: design of flexure hinges*. CRC press, 2002.

[20] J.A.C. Martins, J.T. Oden, and F.M.F. Simes. A study of static and kinetic friction. *Int J Engineering Science*, 28(1), 1990.

[21] David J Meyer, Michael A Peshkin, and J Edward Colgate. Modeling and synthesis of tactile texture with spatial spectrograms for display on variable friction surfaces. In *World Haptics Conference (WHC), 2015 IEEE*, pages 125–130. IEEE, 2015.

[22] Nobuaki Nakazawa, Ryojun Ikeura, and Hikaru Inooka. Characteristics of human fingertips in the shearing direction. *Biological cybernetics*, 82(3):207–214, 2000.

[23] Miguel A Otaduy and Ming C Lin. A perceptually-inspired force model for haptic texture rendering. In *Proceedings of the 1st Symposium on Applied perception in graphics and visualization*, pages 123–126. ACM, 2004.

[24] Todd C Pataky, Mark L Latash, and Vladimir M Zatsiorsky. Viscoelastic response of the finger pad to incremental tangential displacements. *Journal of biomechanics*, 38(7):1441–1449, 2005.

[25] Bo NJ Persson, O Albohr, F Mancosu, V Peveri, VN Samoilov, and Ion Marius Sivebæk. On the nature of the static friction, kinetic friction and creep. *Wear*, 254(9), 2003.

[26] Alexis Prevost, Julien Scheibert, and Georges Debrégeas. Effect of fingerprints orientation on skin vibrations during tactile exploration of textured surfaces. *Communicative & integrative biology*, 2(5):422–424, 2009.

[27] Joseph M Romano and Katherine J Kuchenbecker. Creating realistic virtual textures from contact acceleration data. *IEEE Transactions on Haptics*, 5(2), 2012.

[28] Julien Scheibert, Sébastien Leurent, Alexis Prevost, and Georges Debrégeas. The role of fingerprints in the coding of tactile information probed with a biomimetic sensor. *Science*, 323(5920):1503–1506, 2009.

[29] Lisa Skedung, Katrin Danerlv, Ulf Olofsson, Carl Michael Johannesson, Maiju Aikala, John Kettle, Martin Arvidsson, Birgitta Berglund, and Mark W. Rutland. Tactile perception: Finger friction, surface roughness and perceived coarseness. *Tribology International*, 44(5), 2011.

[30] Allan M Smith, C Elaine Chapman, Mélanie Deslandes, Jean-Sébastien Langlais, and Marie-Pierre Thibodeau. Role of friction and tangential force variation in the subjective scaling of tactile roughness. *Experimental Brain Research*, 144(2):211–223, 2002.

[31] Michael Wiertlewski, Charles Hudin, and Vincent Hayward. On the 1/f noise and non-integer harmonic decay of the interaction of a finger sliding on flat and sinusoidal surfaces. In *Proc. IEEE World Haptics Conference (WHC)*. IEEE, 2011.

[32] Michael Wiertlewski, José Lozada, and Vincent Hayward. The spatial spectrum of tangential skin displacement can encode tactual texture. *IEEE Transactions on Robotics*, 27(3), 2011.

[33] Michael Wiertlewski, José Lozada, Edwige Pissaloux, and Vincent Hayward. Causality inversion in the reproduction of roughness. In *Haptics: Generating and Perceiving Tangible Sensations*. Springer, 2010.

[34] Laura Winfield, John Glassmire, J Edward Colgate, and Michael Peshkin. T-pad: Tactile pattern display through variable friction reduction. In *Proc. World Haptics Conference (WHC)*. IEEE, 2007.

[35] Takashi Yoshioka, James C Craig, Graham C Beck, and Steven S Hsiao. Perceptual constancy of texture roughness in the tactile system. *The Journal of Neuroscience*, 31(48), 2011.